Synthesis of Pure Boron Single-Wall Nanotubes

Dragos Ciuparu,*,† Robert F. Klie,‡ Yimei Zhu,‡ and Lisa Pfefferle†

Department of Chemical Engineering, Yale University, P.O. Box 208286, New Haven, Connecticut 06520, and Center for Functional Materials, Brookhaven National Laboratory, Upton, New York 11973

Received: February 16, 2004; In Final Form: February 27, 2004

We report here the first synthesis of pure boron single-wall nanotubes by reaction of BCl_3 with H_2 over an Mg−MCM-41 catalyst with parallel, uniform diameter (36 ± 1 Å) cylindrical pores. The composition of the tubular structures observed in TEM was confirmed by electron energy loss spectroscopy, and the tubular geometry was confirmed by the presence of the characteristic spectral features in the Raman breathing mode region.

Boron nanostructures have recently attracted much attention because they are predicted to possess special properties superior to those of other one-dimensional nanomaterials. Theoretical studies anticipated that boron nanotubes are stable[1,2] and, independent of structural helicity, have metallic conductivities exceeding that of carbon nanotubes.[3] While synthesis of boron nanotubes has not been previously reported, several studies have focused on the synthesis of boron nanowires. Boron nanowires have been produced by radio frequency magnetron sputtering.[4−10] Both amorphous[11] and crystalline[12] boron nanowires were obtained by laser ablation, while chemical vapor deposition produced crystalline boron nanowires.[13] Here we report the synthesis of single-wall boron nanotubes by reaction of BCl_3 with H_2 over an Mg−MCM-41[14] catalyst with parallel, uniform-diameter (36 ± 1 Å) cylindrical pores. The boron nanotubes produced are approximately 3 nm in diameter, comparable to the diameter of the catalytic template pore, suggesting the nanotube growth is physically constrained by the pores of the mesoporous molecular sieve.

Previously, we have shown that arrays of uniform-diameter single-walled carbon nanotubes can be grown successfully using a cobalt catalyst incorporated into the pore walls of mesoporous silica templates (MCM-41) with a very narrow distribution of pore diameters (±1 Å full width at half-maxima).[15] In this contribution we report the use of such templated technique to grow pure boron nanotubes by using a magnesium-substituted MCM-41 template with a pore diameter of (36 ± 1) Å.

A 6 mm internal diameter quartz reactor was loaded with 200 mg of freshly prepared Mg−MCM-41 template supported in the reactor on an alumina plug. The reactor was placed into an electric furnace and heated under continuous flow of hydrogen to 870 °C. When this steady-state temperature was achieved, 99.9 wt % purity BCl_3 from Air Products and Chemicals, Inc. (10 ppmw of phosgene impurity) was added to the reactor feed and allowed to flow at a BCl_3/H_2 volumetric ratio of approximately 1:6 over the template for 45 min. The total flow rate during reaction was 1.5 L/min (standard temperature and pressure). The reactor was then cooled to room temperature under flowing helium. The material recovered from the reactor showed a grayish color and a significantly higher hardness compared to the fresh Mg-MCM-41 sample, suggesting that metallic boron is embedded in the template material. It should be mentioned here that these reaction conditions are significantly milder than those used in other studies of BCl_3 reaction with hydrogen to form boron films.[16] An experiment performed under identical conditions with the reactor loaded with a pure siliceous MCM-41 catalyst did not produce boron nanotubes, suggesting the magnesium in the Mg−MCM-41 is the catalyst or the catalyst precursor for the growth of single-walled boron nanotubes. The reaction setup was mounted in the fume hood and the unreacted boron trichloride was burnt in a hydrogen flare to prevent releasing the highly toxic boron trichloride into the atmosphere.

The boron-loaded template was ground in an agate mortar, suspended in ethanol, and sonicated for approximately 30 min. Then 0.05 mL of this suspension was dropped on a copper mesh coated with an amorphous holey carbon film, and the ethanol was evaporated prior to transmission electron microscopy (TEM) analysis. The TEM results were obtained using the JEOL-3000F STEM/TEM, equipped with a Schottky field-emission source operated at 300 keV, an ultrahigh-resolution objective lens pole piece (C_s = 0.52 nm), and a postcolumn Gatan imaging filter (GIF) for electron energy-loss spectroscopy (EELS). The microscope and GIF spectrometer were setup for a convergence angle (α) of 11 mrad and a spectrometer collection angle (θ_c) of 24 mrad for scanning transmission electron microscopy (STEM) mode, resulting in a probe size of 1.4 Å. Z-contrast images[17] are formed by collecting the high-angle scattering on an annular detector while the probe is scanned across the specimen. The experimental setup allows us to use low-angle scattered electrons for the elemental analysis using EELS.[18] The information gained by EELS is analogous to the near-edge X-ray absorption spectroscopy (XANES). It is important to note here that although XANES provides a higher energy resolution (<0.1 eV, EELS ∼ 1.0 eV), the lack of spatial resolution does not allow studying individual B-nanotubes on the MCM-41 support.

Figure 1a shows a conventional high-resolution TEM micrograph of a nanotubular structure on the Mg−MCM-41 support, with a tube diameter comparable to the reported pore-size; the initial length of this nanotube outside the pore of the catalyst was determined at 16 nm. These nanotubes were found to be extremely sensitive to high-energy electron beam exposure. Within only a few seconds of exposure to the electron beam,

* Corresponding author. E-mail: dragos.ciuparu@yale.edu.
† Yale University.
‡ Brookhaven National Laboratory.

10.1021/jp049301b CCC: $27.50
Published on Web 03/10/2004

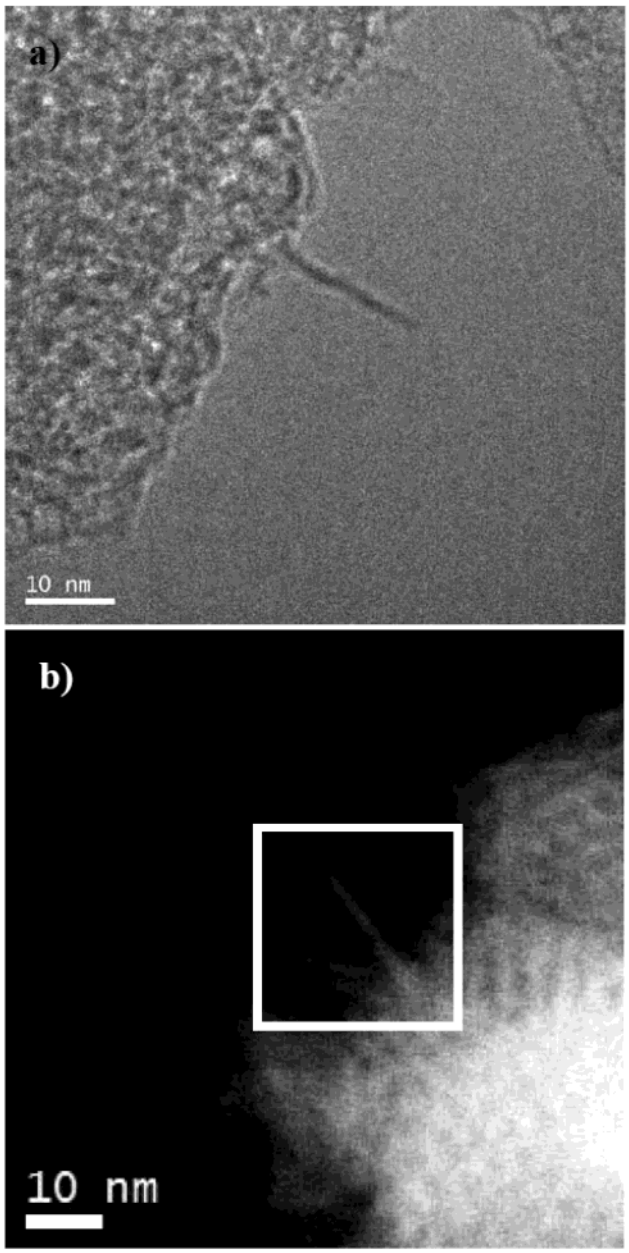

Figure 1. High-resolution image of a boron nanotube with the Mg−MCM-41 template support. (a) A conventional TEM micrograph showing a nanotube of 3 nm diameter and 16 nm length. Due to the extreme beam sensitivity and the charging of the sample, the image appear blurred and out of focus. (b) High-resolution Z-contrast image in STEM mode showing the Mg−MCM-41 support with the regular pore-structure and a supported boron nanotube. The square in this image indicates the area of the electron beam scan to acquire the EELS spectrum.

the length and structure of the tube were changed significantly and the tubes were ultimately destroyed. Hence, for this experiment low-dose techniques had to be used to minimize the exposure of the sample to the electron beam. In addition, the samples were charging under the electron beam, which resulted in vibrations of the exposed sample area and hence to a degraded image quality and resolution. Figure 1b shows Z-contrast image in STEM of a different nanotube, similar in diameter and length to the one shown before. The nanotube appears to have very low contrast compared to the MCM-41 support, which indicates that the tube is significantly thinner and composed of lighter elements than the mesoporous silica support, since the image intensity in the Z-contrast image is

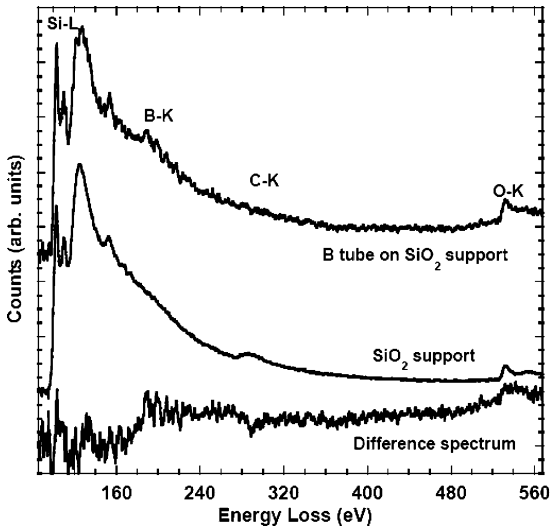

Figure 2. EELS spectrum of the Mg−MCM-support and the area indicated in Figure 1b. Each spectrum is background subtracted and corrected for the multiple-scattering component. The acquisition time for the SiO_2 support spectrum is 3 s, while the spectrum containing the B-nanotube was acquired for 5 s. In addition, the difference between the two spectra is shown.

largely determined by the atomic number (Z) and the thickness of the specimen. The regular pore-structure of the Mg−MCM-41 template can also be clearly recognized in this micrograph.

Due to the high sensitivity of the sample to the electron beam, it is not possible to acquire an EELS spectrum with the electron probe focused on the nanotubes. Instead, we continuously scanned the beam over the area of interest while acquiring an EELS spectrum with a slightly longer exposure time. The resulting spectra are shown in Figure 2, which contains information from both the nanotubes as well as the Mg−MCM-41 support. In addition, we have displayed a spectrum from the MCM-41 template only, which clearly shows the Si−L and O−K core loss edges with the typical fine-structure of amorphous SiO_2, and a small C−K edge peak resulting from the underlying amorphous C-support film. The spectrum taken with an electron probe scanning inside the square in Figure 1b containing the nanotube and the template support, is also shown in Figure 2. Besides the Si−L edge and the O−K edge stemming from the template, this spectrum also shows an increased intensity at an energy of 186 eV. This core-loss edge can be clearly identified as the B−K edge, and the difference spectrum in Figure 2 obtained by subtracting the spectrum of the silica support from that of the boron tube on the silica support shows that the only difference between the two spectra is the presence of the B−K edge, which clearly originated from the nanotubular structure and the absence of the C−K edge, since the structures are suspended over a hole in the amorphous carbon film. Unfortunately, the signal-to-noise ratio of the spectrum from the B-nanotube is too small to reliably analyze the near-edge fine-structure of the B−K edge. Nevertheless, since the only difference between the two spectra is the presence of the nanotube on the MCM-41 support and the presence of the B−K edge, we can conclude that the observed nanotubular structures are clearly pure-boron nanotubes.

The presence of tubular structures has been also confirmed by the presence of spectral features in the Raman breathing mode region at wavenumbers below 500 cm^{-1}. The spectrum shown in Figure 3 was recorded with a catalyst sample removed from the reactor without any purification or pretreatment on a Jobin Yvon Horiba Raman spectrometer equipped with an

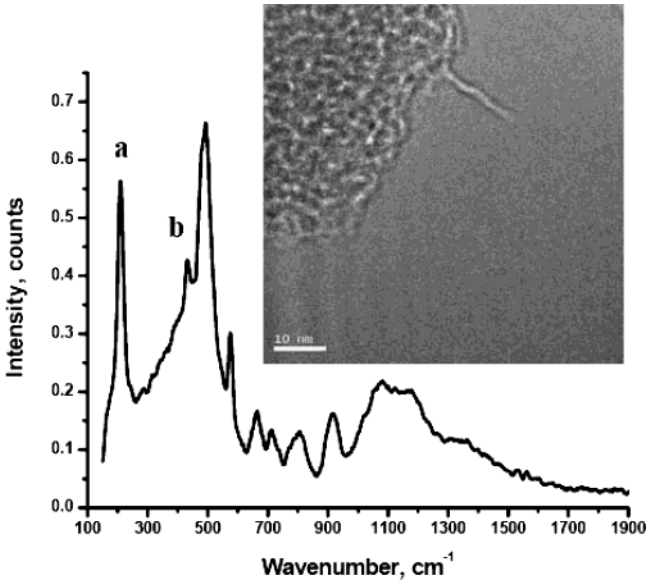

Figure 3. Raman spectra recorded with "as synthesized" single-walled boron nanotubes. A single-walled tubular structure is shown in the inset micrograph.

Olympus confocal microscope using a 532 nm excitation wavelength. The peak at 210 cm^{-1} (labeled a in Figure 3) is typical for tubular structures and corresponds to the characteristic radial breathing mode. The spectral features between 300 and 500 cm^{-1} (peak b) may also be attributed to tubular structures. Similar peaks were reported for single-walled carbon nanotubes.[15] However, because the spectrum recorded for the boron nanotubes sample does not show peaks characteristic for the tangential vibration mode of ordered carbon visible in the 1580−1600 cm^{-1} region, the peak in the Raman breathing mode region belongs to a tubular structure other than carbon. It is not clear yet whether the peaks in the region from 400 to 600 cm^{-1} belong to tubes of smaller diameters or to other boron structures present in our samples. Peaks resulting from the α-boron clusters were observed at 525 cm^{-1} and higher frequencies.[19] The inset in Figure 3 shows a boron nanotube where the single-walled tubular structure is clearly apparent.

Boron nanotubes have been anticipated from ab-initio calculations and their electronic properties predicted, but they have never been reportedly produced. The boron nanotubes produced and characterized in this letter have diameters of approximately 3 nm, thus approximating the pore size of the Mg−MCM-41 template, and a measured length of about 15−20 nm outside the pores of the catalyst. The boron nanotubular structures reported here are extremely beam sensitive, hence at the current stage a more detailed structure analysis to determine the helicity of the tubes or the exact length and diameter appears not to be possible. All of the boron nanotubes that were found in this sample were associated with, or appeared in close proximity to the template support, suggesting that the growth of the nanotubes is initiated at the template support, most likely at the magnesium sites incorporated into the pore walls.

In summary, we have shown that pure boron single-walled nanotubular structures can be grown on a Mg−MCM-41 catalyst and that the nanotube diameter is observed to be approximately that of the pore diameter of the mesoporous molecular sieve template, suggesting physical templating.

Acknowledgment. The authors acknowledge the financial support from NSF through SGER Grant CHE-0335218 (Yale) and by the U.S. Department of Energy, Division of Materials Sciences, Office of Basic Energy Science, under Contract No. DE-AC02-98CH10886 (BNL). We also thank Professor Gary Haller and Sangyun Lim for providing the Mg-MCM-41 sample.

References and Notes

(1) Boustani, I.; Quandt, A. *Europhys. Lett.* **1997**, *39*, 527.
(2) Gindulyte, A.; Lipscomb, W. N.; Massa, L. *Inorg. Chem.* **1998**, *37*, 6544.
(3) Boustani, I.; Quandt, A.; Hernandez, E.; Rubio, A. *J. Chem. Phys.* **1999**, *110*, 3176.
(4) Cao, L.; Zhang, Z.; Sun, L.; Gao, C.; He, M.; Wang, Y.; Li, Y.; Zhang, X.; Li, G.; Zhang, J.; Wang, W. *Adv. Mater. (Weinheim, Germany)* **2001**, *13*, 1701.
(5) Cao, L.; Liu, J.; Gao, C.; Li, Y.; Li, X.; Wang, Y. Q.; Zhang, Z.; Cui, Q.; Zou, G.; Sun, L.; Wang, W. *J. Phys.: Condens. Matter* **2002**, *14*, 11017.
(6) Wang, Y. Q.; Cao, L. M.; Duan, X. F. *Chem. Phys. Lett.* **2002**, *367*, 495.
(7) Cao, L.; Hahn, K.; Wang, Y.; Scheu, C.; Zhang, Z.; Gao, C.; Li, Y.; Zhang, X.; Sun, L.; Wang, W.; Ruhle, M. *Adv. Mater. (Weinheim, Germany)* **2002**, *14*, 1294.
(8) Wang, Y. Q.; Duan, X. F.; Cao, L. M.; Li, G.; Wang, W. K. *J. Crystal Growth* **2002**, *244*, 123.
(9) Wang, Y. Q.; Duan, X. F.; Cao, L. M.; Wang, W. K. *Chem. Phys. Lett.* **2002**, *359*, 273.
(10) Cao, L. M.; Hahn, K.; Scheu, C.; Ruhle, M.; Wang, Y. Q.; Zhang, Z.; Gao, C. X.; Li, Y. C.; Zhang, X. Y.; He, M.; Sun, L. L.; Wang, W. K. *Appl. Phys. Lett.* **2002**, *80*, 4226.
(11) Meng, X. M.; Hu, J. Q.; Jiang, Y.; Lee, C. S.; Lee, S. T. *Chem. Phys. Lett.* **2003**, *370*, 825.
(12) Zhang, Y.; Ago, H.; Yumura, M.; Komatsu, T.; Ohshima, S.; Uchida, K.; Iijima, S. *Chem. Commun. (Cambridge, United Kingdom)* **2002**, 2806.
(13) Otten, C. J.; Lourie, O. R.; Yu, M.-F.; Cowley, J. M.; Dyer, M. J.; Ruoff, R. S.; Buhro, W. E. *J. Am. Chem. Soc.* **2002**, *124*, 4564.
(14) Beck, J. S.; Vartuli, J. C.; Roth, W. J.; Leonowicz, M. E.; Kresge, C. T.; Schmitt, K. D.; Chu, C. T. W.; Olson, D. H.; Sheppard, E. W.; et al. *J. Am. Chem. Soc.* **1992**, *114*, 10834.
(15) Ciuparu, D.; Chen, Y.; Lim, S.; Haller, G. L.; Pfefferle, L. *J. Phys. Chem. B* **2004**, *108*, 503.
(16) Park, C. S.; Yoo, J. S.; Chun, J. S. *Thin Solid Films* **1985**, *131*, 205.
(17) Browning, N. D.; Chisholm, M. F.; Pennycook, S. J. *Nature* **1993**, *366*, 143.
(18) Egerton, R. F. *Electron Energy-Loss Spectroscopy in The Electron Microscope*; Kluwer Academic Publishing: Norwell, MA, 1986.
(19) Beckel, C. L.; Yousaf, M.; Fuka, M. Z.; Raja, S. Y.; Lu, N. *Phys. Rev. B: Condens. Matter Mater. Phys.* **1991**, *44*, 2535.